Journal of Structural Geology 156 (2022) 104556

Contents lists available at ScienceDirect

Journal of Structural Geology

journal homepage: www.elsevier.com/locate/jsg

Discrete fracture network (DFN) modelling of a high-level radioactive waste repository host rock and the effects on its hydrogeological behaviour

Emese Tóth *, Ervin Hrabovszki, Félix Schubert, Tivadar M. Tóth

Department of Mineralogy, Geochemistry and Petrology, University of Szeged, 6722, Szeged, Hungary

ARTICLE INFO

Keywords:
DFN modelling
Claystone
Flow zone indicator
Fracture aperture calibration
Radioactive waste repository

ABSTRACT

Fracture network modelling and a hydrological evaluation were performed in a well more than 900 m deep that penetrated the Boda Claystone Formation, a potential host rock for high-level nuclear waste disposal facilities in Hungary. The fracture network geometry was generated with a discrete fracture network algorithm, in which the permeability and porosity of the system can be calculated if the aperture of the fractures is known. The hydrological aperture of the fractures was estimated via an aperture calibration based on a comparison of the measured and modelled permeability values. Flow zone indices were calculated for numerous sections along the well, designating hydraulic units, in which the fluid flow-controlling properties are internally even.

Based on the fracture network geometry and the hydraulic flow units, most parts of the well behave uniformly, while three narrow zones differ significantly. The first zone is located in the upper 100 m of the well probably formed due to weathering. The second zone is located at approximately 400 m, where a large-scale structural boundary is presumed. In the third zone at 700 m, a lithological change greatly affects the hydrological properties, but the influence of tectonic processes cannot be ruled out.

1. Introduction

The potential host rock for the high-level radioactive waste repository of Hungary is the late Permian Boda Claystone Formation (BCF), which is located in the Western Mecsek Mountains, SW Hungary (Konrád and Hámos, 2006). The characteristics of this claystone provide good retentive properties, and its low porosity and permeability can prevent the leakage of radionuclides (Krauskopf, 1988; Árkai et al., 2000). In this lithology, significant fluid pathways can exclusively form along planes of structural inhomogeneities and fractures (Anders et al., 2014). Therefore, the investigation of the fracture network geometry and its hydrodynamic behaviour is crucial in understanding the hydrodynamic behaviour of otherwise impermeable rock bodies. Vital areas of study include the connectivity of the fracture system, whether or not single fractures form communicating networks, and the size and location of all potential fracture clusters.

The size of hydrologically active fractures is usually within the resolution of seismic data but transcends the resolution of well log and microstructural studies (Paillet et al., 1993; Childs et al., 1997). Therefore, little information is available about the behaviour of fracture systems at the reservoir scale. Since fracture networks can be approximated as scale-invariant geometrical objects, structural data measured at microscales can be upscaled to larger dimensions (Turcotte, 1992; National Research Council, 1996). Such a discrete fracture network (DFN) modelling approach requires quantitative geometric data of the fracture network, such as the fracture size distribution, spatial density of fracture midpoints, and orientation (dip and dip direction). The essential features of the fractured rock body, such as the connectivity tendency of single fractures as well as the hydrodynamic behaviour of the system (fractured porosity and permeability), can be investigated using simulated models (M. Tóth and Vass, 2011).

This paper aims to characterise the fracture network geometry and the hydrodynamic behaviour of the surroundings of the deepest well (BAF–2) in the BCF using fracture network modelling and evaluating hydraulic measurements in the well.

2. Geological setting

The late Permian BCF is located in SW Hungary (Fig. 1) and is a member of the 4000–5000 m thick Palaeozoic–Triassic sedimentary sequence of the Western Mecsek Mountains. The formation consists of well-compacted reddish-brown claystone, siltstone, and albitolite

* Corresponding author.
E-mail address: tothemese@geo.u-szeged.hu (E. Tóth).

https://doi.org/10.1016/j.jsg.2022.104556
Received 10 September 2021; Received in revised form 14 February 2022; Accepted 19 February 2022
Available online 24 February 2022

(authigenic albite >50%) with dolomite and sandstone intercalations. The main rock-forming minerals are quartz, albite, illite-muscovite, chlorite, calcite, dolomite, and haematite (Árkai et al., 2000; Máthé, 2015). The maximal thickness of the formation is more than 1000 m and the distribution area is approximately 150 km^2 (Konrád and Hámos, 2006). The BCF was deposited in an alkaline lake environment on a periodically drying playa mudflat in an arid to semiarid climate (Árkai et al., 2000; Varga et al., 2005, 2006; Varga, 2009; Konrád et al., 2010).

The study area is located around the subvertical profile of the BAF–2 well, which penetrated the formation in largest thickness of more than 900 m, with close to 100% core recovery. The well intersected characteristic reddish-brown, intensely tectonised claystone. The average dip direction of the bedding in the well is SE-SSE, and the dip is 40° based on acoustic borehole televiewer (BHTV) observations (Bernáth et al., 2014; Konrád et al., 2015).

The grain size gradually increases with depth (claystone - siltstone - fine sandstone). Above the Permian sequences, the BAF–2 well penetrated Quaternary (Holocene, Pleistocene) sediments between 0 and 9.10 m (reported depths are in the total measured depth in metres throughout the paper; Fig. 2A). Between 9.10 and 130 m, reddish-brown claystone with interbedded siltstone is the dominant rock type. This section is intensively weathered; presumably, the rock body was uncovered for an extended period of time in a warm and humid climate before and during the Miocene (Konrád et al., 2015). Limonite, smectite and chlorite-smectite are present as significant alteration products in the uppermost 100 m of the well (Konrád et al., 2015; Máthé, 2015; Németh et al., 2016). The section between 130 and 757 m consists of reddish-brown claystone with siltstone beddings. Between 148.59–153.90 and 233.36–238.40 m, the well crosscuts two thick reductive layers; in these intervals, the sequence contains greenish-grey claystone (Fig. 2A). Presumably, these layers represent two independent reductive events. Based on the interpretation of the BHTV data, the tectonic repetition of the same horizon cannot be ruled out either (Bernáth, 2015; Konrád et al., 2015). The first fine sandstone layer of significant thickness appears at 757.96 m. Below this horizon, the transition zone of the BCF to its coarser-grained bedrock is identified. In this interval, claystone with numerous siltstone and fine sandstone intercalations is the dominant rock type (Fig. 2A; Konrád et al., 2015).

Numerous subsequent tectonic phases could characterise the evolution of the area. Significant NE–SW shortening during the Late Cretaceous (Benkovics et al., 1997) was followed by events related to the formation of the Pannonian Basin in the Neogene. Deformation due to tensional stresses in the early Miocene (Bergerat and Csontos, 1988; Csontos and Bergerat, 1992; Fodor et al., 1999) was followed by late Miocene (Sarmatian) compression (Sebe, 2017) and by thermal subsidence of the basin afterwards (Pannonian; Csontos et al., 2002; Maros et al., 2004). The most recent essential event is the ongoing tectonic inversion of the basin (Konrád and Sebe, 2010).

Konrád et al. (2015) suggest a structural boundary at approximately 400 m in the BAF–2 well. Below this depth, the graded bedding style changes from normal to inverse, and thinning of the graded sequences is observed. In this segment, the sequence contains numerous smaller strata interpreted as overturned.

Many geophysical well logs show a characteristic difference between the upper (0–400 m) and lower (400–915 m) parts of the well. The most significant deviation is shown in the sonic log (Fig. 2B), where the acoustic wave velocity drastically decreases below 400 m (Bernáth et al., 2014). This log indicates the mechanical properties of the rock body by measuring how fast the acoustic waves can travel through the rock body. Based on all this information, the current structural interpretation of Konrád et al. (2015) suggests that the BAF–2 well intersected a tilted fold sheared by fault zones.

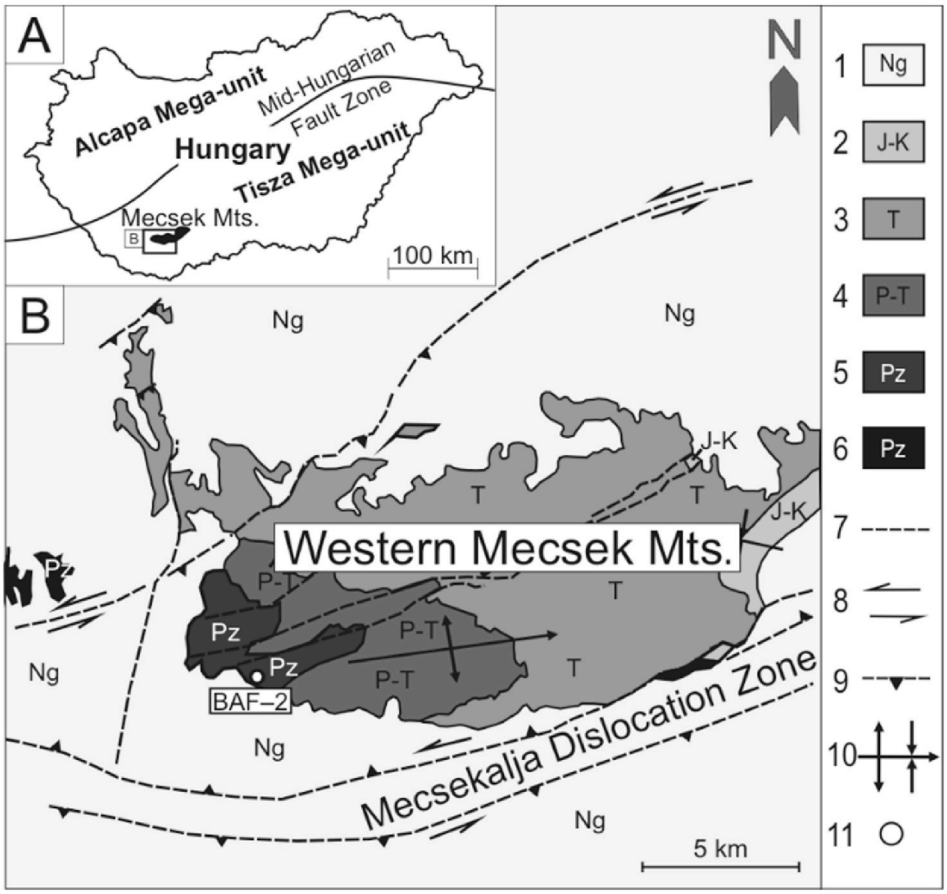

Fig. 1. (A) Map of Hungary with the location of the Mecsek Mountains. (B) Geological map of the Mecsek Mountains with the distribution of the Boda Claystone Formation (modified after Konrád and Sebe, 2010)
Legend: 1, Neogene sediments; 2, Jurassic and Cretaceous sediments and Cretaceous volcanic rocks; 3, Triassic sediments (sandstones, carbonates and evaporites); 4, Upper Permian–Triassic Kővágószőlős Sandstone Fm; 5, Upper Permian Boda Claystone Fm; 6, Palaeozoic; 7, fault; 8, strike-slip fault; 9, thrust fault; 10, syncline and anticline; 11, well site.

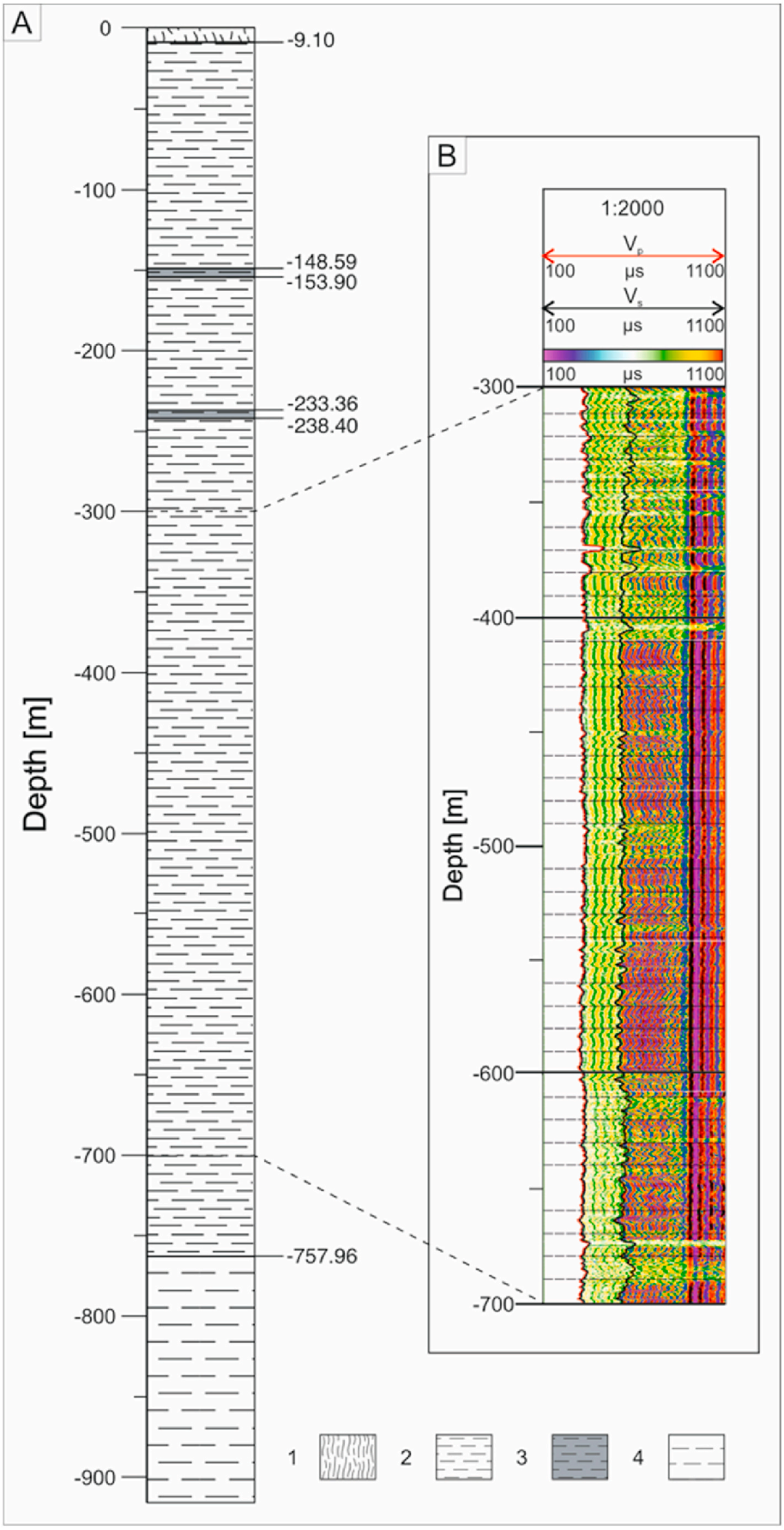

Fig. 2. (A) Lithology log of the BAF–2 well; 1, soil, loess; 2, claystone with siltstone beddings; 3, greenish-black reductive claystone; 4, claystone with siltstone and sandstone beddings (modified after Hrabovszki et al., 2017). (B) Sonic log for the BAF–2 well between 300 and 700 m. Red line indicates the travel time of the primary waves, black line indicates the travel time of the secondary waves (modified after Bernáth et al., 2014). (For interpretation of the references to colour in this figure legend, the reader is referred to the Web version of this article.)

Previous studies distinguished four vein generations along the BAF–2 well that indicate multiple tectonic and/or diagenetic processes (Hrabovszki et al., 2017, 2020, 2022; Tóth et al., 2020). The veins are classified into the following categories: branched veins, straight veins, *en echelon* vein arrays, and breccia-like veins. In the BAF–2 well, the average dip values of the vein types are 42° (branched veins), 70° (straight veins), and 22° (*en echelon* vein arrays) (Hrabovszki et al., 2017). All four vein generations occur all along the rock body. The fractures are filled predominantly with calcite, anhydrite, and barite-celestine (Árkai et al., 2000; Hrabovszki et al., 2020, 2022; Tóth et al., 2020).

Accurate knowledge of hydrogeological conditions is an essential requirement for assessing the suitability of a geological formation for the storage of radioactive waste. The general hydrogeological conditions of the Western Mecsek Mountains are determined by the morphology of the mountains and their surroundings. The Palaeozoic–Mesozoic formations of the mountains rise 400–500 m from their surroundings, defining a regional recharge zone whose discharge areas are the Neogene basins located in its wider periphery (Csicsák, 1999).

Due to its petrophysical properties and thickness, the BCF is an aquiclude. Due to its high clay content, fracture self-sealing is also a frequent phenomenon (Csicsák, 1999). In its surface outcrops, the rock body is relatively well fragmented and significantly weathered; therefore, groundwater amounts can be significant in the uppermost 40–50 m. Based on hydraulic testing of the well, transmissivity decreases with depth; however, high-transmissivity zones also occur, even in the deeper parts (down to approximately 500 m). The well can be divided into two parts based on the transmissivity log. High-transmissivity zones occur mainly in the upper 500 m, while below 500 m, the transmissivity is close to constant at a significantly reduced value throughout the well. The highest value is 1.9×10^{-5} m^2/s, while the lowest value is 2.7×10^{-12} m^2/s (Fig. 3; Andrássy et al., 2018).

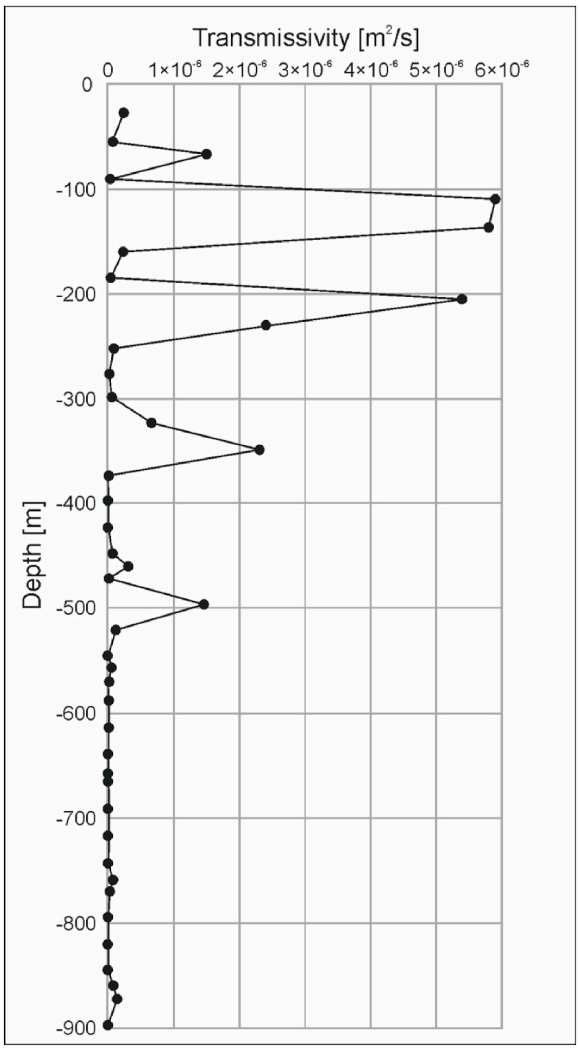

Fig. 3. Transmissivity log of the BAF–2 well based on well-hydraulic testing (Andrássy et al., 2018).

3. Methods

Fracture networks usually follow a fractal-like pattern independent of the lithology and structural evolution (Barton and Larsen, 1985; La Pointe, 1988). Such an appearance allows fracture networks to be modelled at any scale using measured geometric data. In this study, a discrete fracture network (DFN) modelling approach was used to predict the hydrodynamic behaviour of the rock body based on the geometric data of the individual fractures (Witherspoon et al., 1980; Neuzil and Tracy, 1981; Zimmerman and Bodvarsson, 1996).

DFN modelling has two consecutive steps. First, the geometric parameters of the individual fractures must be determined. These parameters serve as the foundation for the simulation. The most important geometric parameters and those used in the modelling are the fracture length distribution, the spatial density of fracture midpoints, the orientations of the fractures, and their aperture. Second, the network is generated using a fracture modelling software program. In this study, the discrete fracture network modelling system called Infress (previously RepSim) was applied (M. Tóth et al., 2004; M. Tóth, 2010; M. Tóth, 2018).

3.1. Determination of the geometric parameters of fractures

Fracture size is one of the essential geometric parameters of DFN modelling. Numerous studies have shown that the distribution of fracture lengths follows a power-law function so that

$$N(L) = F^{*}L^{-E} \quad (1)$$

where N(*L*) is the number of fractures with a length of *L* and E and F are the parameters of the distribution function (Yielding et al., 1992; Min et al., 2004). This asymmetric distribution denotes that the number of small fractures is significantly larger than the number of large fractures.

Measurement of fracture length cannot be easily performed on cores because most individual fractures do not terminate within the core. To solve this problem, M. Tóth (2010) introduced a novel algorithm. Here, two images with different sensitivities are required to determine the length exponent (E in Eq. (1)). The number of fractures identified by the less sensitive method is necessarily less than the number of fractures seen by the more sensitive method, with a constant difference (ΔN(*L*)). Using this difference and the detection limits of the applied methods, the parameters of Eq. (1) can be calculated. For further details, see M. Tóth (2010). In our study, the length exponent was determined by comparing BHTV data (lower resolution) and core images (higher resolution) with image analysis. The images of the cores were taken with a Nikon D90 camera with a lens of 100 mm focal length and an aperture setting of f/8 under constant ambient light conditions. The vertical resolution of the BHTV is 4 mm, while the resolution of the core images is 1 mm.

The spatial density of the fracture network can be defined by the fractal dimension of the fracture pattern. In a borehole, the real fracture network is crosscut by a line (defined by the well itself), resulting in a point series. In this case, the spatial density of the fractures can be characterised by computing the fractal dimension of this series. As the borehole image logs (e.g., BHTV) define the exact spatial position of fractures, the intersection points between the fracture network and the borehole can be interpreted as the point process in question. The fractal dimension of this pattern was calculated using rescaled range (R/S)

analysis, which aims to estimate the Hurst exponent. The degree of self-similarity is defined by the Hurst exponent (H) parameter, which is directly related to the fractal dimension so that:

$$D = 2 - H \tag{2}$$

The parameter H was determined for each 100 m interval with an overlap of 50 m (0–100 m, 50–150 m, 100–200 m, etc.) along the well using Benoit 1.0 software following the approach introduced by M. Tóth (2010). In addition to the fractal dimension, another commonly used parameter that may also characterise the fracture density is the P10 parameter (number of intersections per metre), which was also calculated and plotted with depth. The orientations of the fractures were described by the dip direction and dip angle obtained from the BHTV data.

3.2. Fracture network modelling and aperture calibration

The fracture network of the investigated well was generated in 3D by Infress fracture network modelling software (M. Tóth, 2010; M. Tóth and Vass, 2011; Bauer and M. Tóth, 2017). This DFN software package simulates single penny-shaped fractures in a stochastic manner with the given geometric parameters of the fracture network. Infress generates the desired number of equally probable realisations of the fracture network geometry. A subroutine of the software code enables the investigation of the size and spatial position of the communicating subsystems of the simulated fracture networks (M. Tóth and Vass, 2011). Based on the fracture network geometry and an aperture value for all fractures, the fractured porosity and the intrinsic permeability tensor elements can be computed for any cubic volume element of the modelled rock body. The algorithms and the mathematical background of the software code are described in detail by M. Tóth, (2018).

Determining and even defining the fracture aperture are somewhat problematic (Vermilye and Scholz, 1995; Keller, 1998; Liu, 2005; Bisdom et al., 2016). The physical aperture is usually defined as the average distance between the opposite walls of the fracture that can be measured using an image analysis approach at any scale. In hydrodynamic processes, the hydraulic aperture should be used instead, which is defined as a theoretical conduit that produces the same flow rate as the real fracture (Olsson and Barton, 2001; Cheng et al., 2020).

Furthermore, the fracture aperture should not be defined as an independent geometric parameter. It usually follows a power-law distribution function, similar to the fracture length, and a tight linear correlation can be assumed between the two parameters based on numerous studies (Barton and Larsen, 1985; Pollard and Segall, 1987; Gudmundsson et al., 2001):

$$a = A^{*}L \tag{3}$$

where a is the aperture, the aperture coefficient A is characteristic of the rock body, and L is the length of the fracture, which is the diameter of a theoretical penny-shaped fracture in the model. In many different rock types, the ratio of the maximal aperture to the length varies within approximately 2×10^{-3}–8×10^{-3} for joints and 3×10^{-3}–3×10^{-2} for shear fractures (Opheim and Gudmundsson, 1989; Vermilye and Scholz, 1995). Using this simple correlation, the initial aperture for every fracture with the modelled length can be computed. Finally, the modelled fractured porosity and permeability values estimated for any cubic cell depend exclusively on the fracture network geometry and the aperture coefficient (A).

The initial aperture of a fracture can be modified by numerous water-rock interaction processes, which can have different effects on the initial aperture from part to part along the fracture plane (Vermilye and Scholz, 1995). In addition, the aperture is affected by the prevailing stress field, fracture orientation, depth and roughness of the fracture wall (Kumar et al., 1991; Liu, 2005). Therefore, the current hydraulic fracture aperture is the result of numerous independent processes that make it difficult to estimate. Choosing reliable aperture values, nevertheless, is essential in the evaluation of the hydraulic conductivity behaviour of a fractured rock body.

Given the simulated fracture network geometry and the measured transmissivity data, the hydraulic aperture can be estimated by comparing the observed and modelled permeabilities following the algorithm outlined in Fig. 4.

Infress software, as mentioned above, allows the calculation of the porosity (φ_{ini}) and the 3x3 intrinsic permeability tensor for any cubic cell based on the generated fracture network geometry using an aperture coefficient value. As hydraulic measurements of a well do not account for the anisotropy of permeabilities, hereafter, the mean of the diagonal elements of the permeability tensor (k_{ini}) is used during calibration.

Based on the measured transmissivity data, the observed permeability (k_{obs}; Fig. 4) can be calculated. The transmissivity for the horizontal flow of a rock layer with a specified thickness of d is:

$$T = K^{*}d \tag{4}$$

where T is the transmissivity and K is the hydraulic conductivity. The d value in Eq. (4) is the packer interval used for the transmissivity measurement. From the hydraulic conductivity, permeability is defined as:

$$K = \frac{k\varrho g}{\eta} \tag{5}$$

where ϱ and η are the density and the dynamic viscosity of the fluid, respectively, g is the gravitational acceleration, and k is the permeability of the rock body (Grant, 2005). The density and dynamic viscosity of the water were taken as unity in the equation. In this way, the observed permeability (k_{obs}) can be determined for any interval where transmissivity was measured.

In our study, the hydraulic aperture (a_{hyd}) of the fractures was obtained using the above aperture calibration approach (Fig. 4). The objective of aperture calibration is to change the aperture coefficient value (A) so that the two permeability values (k_{ini} and k_{obs}) for the same volume become equal. To estimate permeability tensor elements with Infress, a rock volume of d^3 was considered. In this way, an average aperture coefficient could be computed for each interval independently, allowing the effective porosity to be calculated for all sections.

The hydrodynamic characteristics of any rock body can be described using the flow zone indicator (FZI). This parameter is based on the covariation of porosity and permeability and is usually used to evaluate reservoir quality. This index can also be applied to define flow units, volumes of reservoirs in which the geological and petrophysical properties that control the fluid flow are internally consistent (Amaefule et al., 1993). According to Al-Dhafeeri and Nasr-El-Din (2007), FZI can be calculated as:

$$FZI = \frac{RQI}{NPI} = \frac{0.0314\sqrt{\frac{k}{\Phi}}}{\frac{\Phi}{(1-\Phi)}} \tag{6}$$

where FZI is the flow zone indicator in μm, NPI is the normalised porosity index, RQI is the reservoir quality index, k is the permeability in mD, and Φ is the porosity in a volume fraction. FZI values are related to the porosity, permeability, capillary pressure, lithology distribution, mineralogy, and sedimentary structures and are also affected by diagenetic processes (Dezfoolian, 2013). Various combinations of these factors may result in distinct rock hydraulic flow units (HFUs). A HFU, by definition, is a volume of a rock body where the geological and petrophysical properties that control the fluid flow are internally consistent (Amaefule et al., 1993). It is worth noting that elevated FZI values do not necessarily mean better hydraulic conductivity; high values indicate only the changing relationship between porosity and permeability. For example, FZI can increase with increasing permeability due to fracturing; if the porosity does not grow to the same extent or if porosity

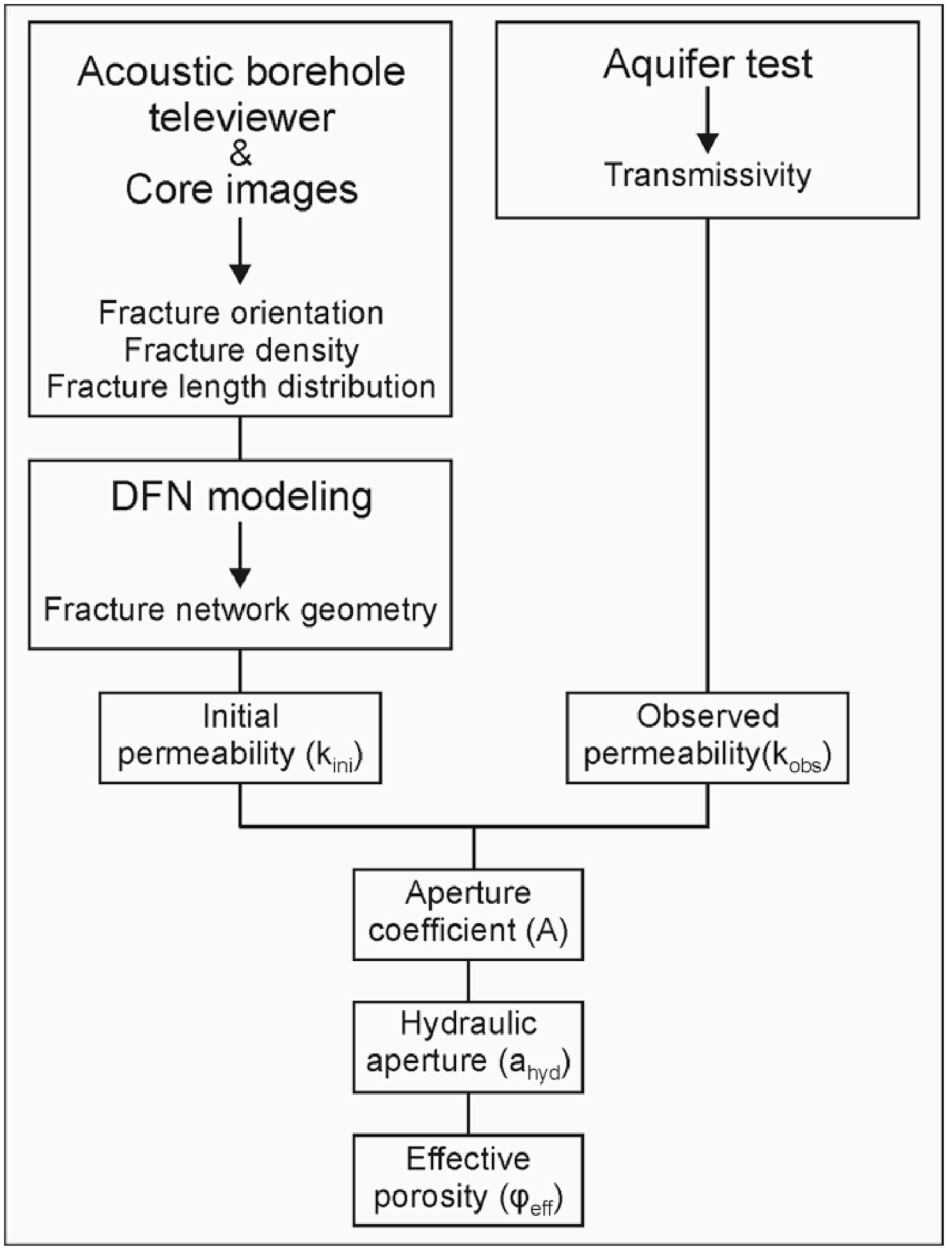

Fig. 4. Flow chart of the algorithm for determining the hydraulic properties of the BAF–2 well. Aperture coefficient, hydraulic aperture and effective porosity of the well are extracted from the modelled fracture network geometry and the well-hydraulic transmissivity measurement.

drops without a significant decrease in permeability, FZI may also increase.

4. Results

4.1. Fracture network parameters

Fracture density can be defined in many different ways. The number of fractures per metre index (P10) was calculated for every 100 m with 50 m overlap based on the BHTV data (Fig. 5A). This calculation includes all planes detected by BHTV, including faults, veins, joints and bedding planes. The upper part of the well, between 100 and 420 m, is highly fractured; the average fracture density is 9–10 m^{-1}. Below 420 m, three fractured zones can be distinguished at ~500, ~650, and ~850 m (5–6 m^{-1}). The fracture density between these zones is low; 3–4 fractures per metre can be found in the least fractured sections (Fig. 5A).

The fractal dimension (D) was calculated for 100 m long sections of the well with 50 m overlap. The average D is 1.37 ± 0.05, while high D values characterise three well-defined zones, 140–250, 580–680 and 790–870 m, with elevated fracture densities (Fig. 5B). A single length exponent (E) and an F parameter were calculated for the entire well using the approach detailed by M. Tóth (2010): E = −0.90 and F = 10.00.

Based on the BHTV evaluations, most planes detected in the borehole have an SSE dip direction (Fig. 6) with an average orientation of ~ N162° E−60°. The planes in this group primarily indicate sedimentary bedding and probably fracture planes parallel to layering (Fig. 6).

4.2. Fracture network modelling

Modelling was carried out in a 150 × 150 × 925 m cuboid surrounding the well. The presence of connected subsystems can characterise the simulated fracture networks in each run. Based on the above-mentioned fracture network parameters and 20 independent runs, five

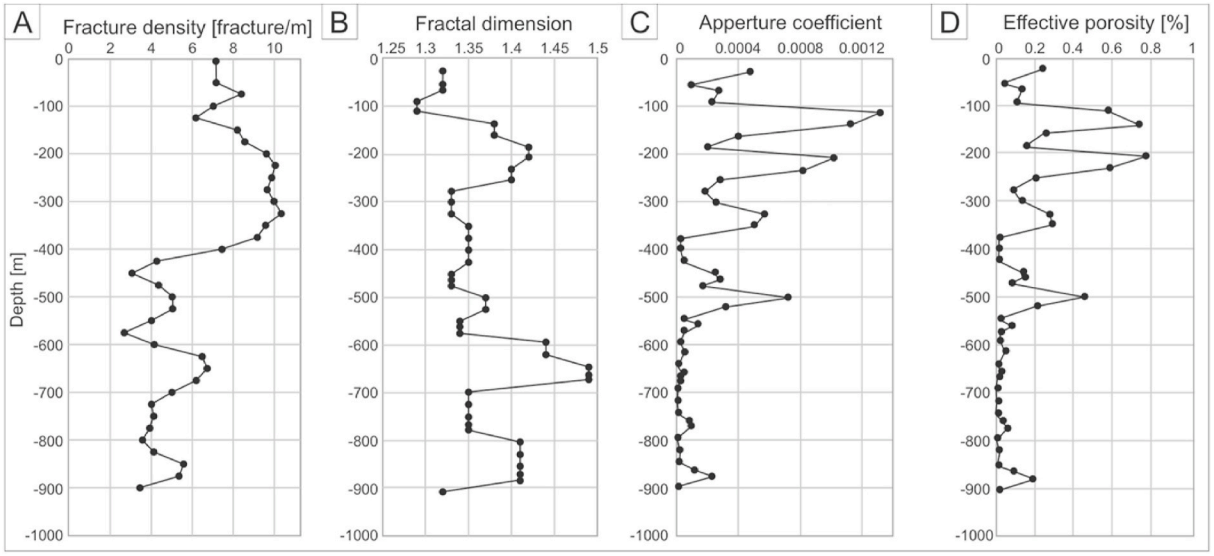

Fig. 5. (A) Fracture density log of the well expressed with the number of fractures per meter (P10 parameter); (B) Fractal dimension log of the well, determined in every 100 m, with 50 m overlap; (C) Variation in aperture coefficient along with the well; (D) Effective porosity log of the well.

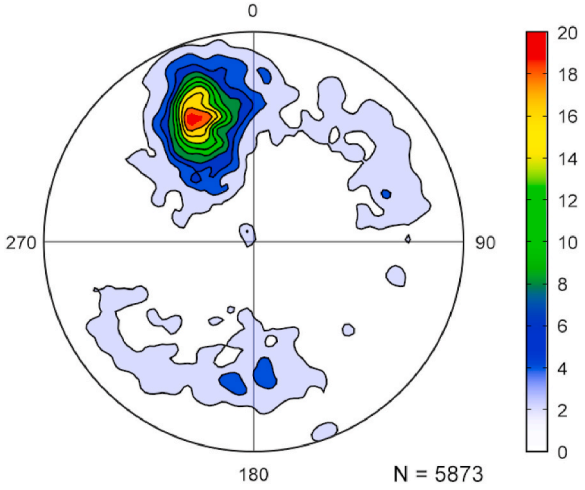

Fig. 6. Lower-hemisphere and equal-area projections of the poles of the bedding and fracture planes based on BHTV data on Schmidt net. The isolines denote a 2% increase in frequency. The largest group of planes has a SSE dip direction, which coincides with the dip direction of the bedding planes.

typical geometries were distinguished regarding the communication of the fracture network (Fig. 7).

In the first case, the whole fracture system defines one communicating group (Fig. 7A). In many cases, two connected subsystems are present that do not interconnect with each other. The boundaries between the subgroups vary from one run to another and appear at ~300, ~400 or ~700 m (Fig. 7B, C, D). In some cases, the fracture system of the well splits into four connected fracture subgroups along the boundaries at ~100, ~400, and ~700 m (Fig. 7E).

4.3. Estimation of the aperture coefficient and effective fractured porosity

The values of the calibrated aperture coefficient (A in Eq. (3)) of the 20 m long intervals, from which the transmissivity data were obtained, decrease with depth and vary between 4×10^{-6} and 8×10^{-4} (Fig. 5C). The hydraulic aperture of a fracture with a diameter of 1 m may change between 4 μm and 0.8 mm, depending on the influence of the post-tectonic fluid-rock interaction processes, the degree of closure with depth and the current stress field. The aperture coefficient of the fracture system in the lower half of the well is significantly reduced in two sections (380–420 m and 580–850 m), while the upper section (120–160, 200–240 and 320–340 m) is characterised by elevated values.

The effective porosity log (Fig. 5D) follows the anomalies seen on the aperture coefficient log (Fig. 5C). Sections with a high effective porosity are characteristic in the upper part of the well (above 400 m). There are two sections with significantly higher porosity values in the lower part at ~500 m and ~850 m, while a small increase can be detected at ~780 m (Fig. 5D).

4.4. Poro-perm diagram and the flow zone indicator

The examination of the porosity and permeability data together allows the characterisation of the reservoir bodies from a hydrodynamic point of view. Therefore, the conventional porosity-permeability (abbreviated as poro-perm hereafter) diagram was constructed, and FZI values were calculated for all 44 data points along the well. The permeability data were derived from hydraulic measurements of the well, while the porosity data were estimated based on the DFN model and the calibrated aperture coefficients. The largest section of the well follows the same trend on the poro-perm diagram with an excellent fit ($R^2 = 0.986$; Fig. 8A, black curve). In this section the typical value of the FZI is between 200 and 350 (Fig. 8C/b, d, f). There are three narrow, distinct zones with elevated FZI values (60–110 m, 350–420 m, and 690–770 m; Fig. 8C/a, c, e). The data points for all of these sections lie on the same trend on the poro-perm diagram ($R^2 = 0.977$; Fig. 8A, orange curve). Using the poro-perm trends and the FZI values, the studied well can be subdivided into six hydraulic flow units (Fig. 8B and C).

5. Discussion

5.1. Evaluation of the structural elements of the well

This study examines the fracture network of a potential high-level radioactive waste repository site in Hungary using fracture network modelling. The modelling parameters were determined primarily using BHTV data and core images of the BAF–2 well. A BHTV records fracture planes and bedding similarly along the borehole; both appear as sinusoidal curves in the images. Although several steep fractures crosscut the studied formation, many others lie parallel to the bedding surfaces (Konrád et al., 2015). This geometry suggests that due to competence

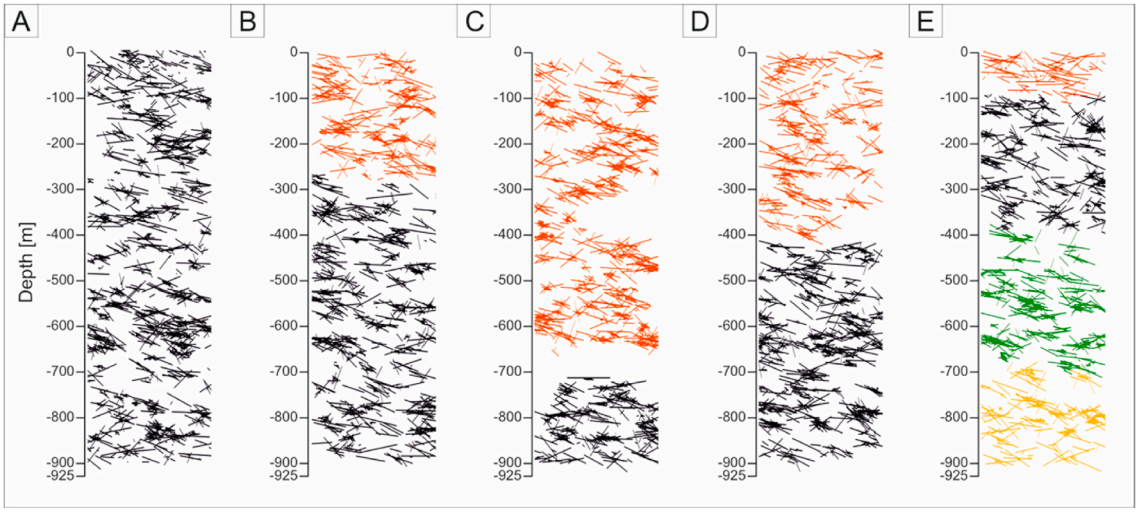

Fig. 7. Vertical east-west sections of typical simulated fracture network geometry patterns (A–E) of the BAF–2 well based on 20 independent runs. Different colours indicate the communicating fracture groups within the well. The width of the sections is 150 m. (For interpretation of the references to colour in this figure legend, the reader is referred to the Web version of this article.)

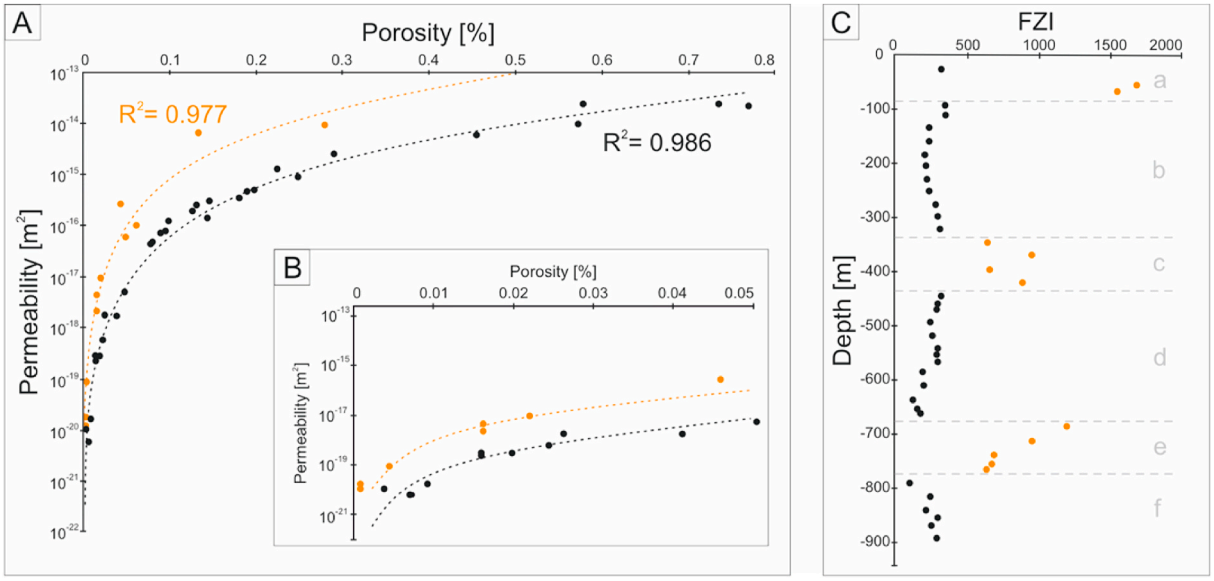

Fig. 8. (A) Poro-perm trends of the BAF–2 well based on the measured permeability and computed effective porosity data. (B) Inset of the poro-perm trend diagram of small values. (C) The hydraulic flow units of the BAF–2 well are indicated by the flow zone indicator (FZI), dashed lines designate the borders of the HFU-s, grey letters (a–f) indicate the HFU-s. Different colours indicate different FZI trends. (For interpretation of the references to colour in this figure legend, the reader is referred to the Web version of this article.)

contrast these planes were most effectively deformed during tectonic or atectonic events. Consequently, fractures and stratifications are difficult to distinguish using BHTV images in the lithologically homogeneous sections of the rock body. On the other hand, fractures and bedding planes may play an identical hydrodynamic role, as they all may act as migration pathways for water and radionuclides. Therefore, for modelling purposes, we took into account every discontinuity within the rock body detected by the BHTV. Therefore, the results of the fracture network modelling approach outline the worst-case scenario regarding the hydraulic features and fracture connectivity of the studied rock body, which is a potential host rock for the repository of high-level radioactive waste.

5.2. Fracture density of the well

Two numerical indices were used to characterise the fracture intensity of the formation: the number of fractures within a metre (P10 index) and the fractal dimension. Based on both indicators, the well can be subdivided into two major sections with a boundary at approximately 400 m. The fracture density (P10 log) characteristics differ significantly between the lower and upper sections of the well; a well-defined, sharp boundary horizon can be drawn between them. Several factors can affect the fracture density of a rock body, among which the rock type, grain size, prevailing stress field and tectonic events are the most essential. In the BAF–2 well, the average grain size of the sediment continuously increases downwards without any abrupt jump at 400 m, and no significant change in lithology can be detected at this depth. Any discontinuous change along this boundary in either the thickness or the lithology of the beds could influence the fracture pattern. Furthermore, both the average grain size and the diagenetic history of the various rock types might result in different rheological properties, causing diverse rock bodies to respond differently to the same stress field (Brace and

Riley, 1972; Paterson, 1978). Even a slight change in the petrophysical features of the rock could influence the fracture density (National Research Council, 1996). Therefore, it cannot be excluded that the change in the fracture pattern at 400 m is caused by the increasing average grain size and thus the difference in the rheological parameters of the formation.

On the other hand, based on stratigraphic irregularities, such as overturned beds and changes in graded sequences, some authors have suggested the presence of a structural boundary in the well (Konrád et al., 2015). This assumption is also supported by the acoustic wave velocity log, which shows an abrupt change in the rock body at 400 m (Bernáth et al., 2014).

In the lower part of the borehole, sandstone layers are more common towards the bedrock below 757 m, where the first sandstone layer with a significant width appears. Here, the density of fractures (P10 index) decreases simultaneously with the presence of sandstone layers (Fig. 5A), further strengthening the correlation between the fracture geometry and the grain size of the host rock.

Alternatively, instead of changing of the rock type, the three highly fractured zones in the lower half of the well may indicate three distinct shear zones determined by the prevailing stress field. In this model, poorly deformed horizons separate the shear zones at 580 and 710 m.

5.3. Hydrological evaluation of the fracture network

The aperture coefficient, which is the aperture of a fracture of unit size, significantly influences the hydrological behaviour of fractured rock bodies. Its value continuously decreases downwards with intervals of anomalous behaviour. The coincident scattering of the hydrological aperture may be the consequence of diverse water-rock interaction processes such as dissolution and cementation. The reduction in the aperture coefficient along the borehole coincides with more closed, presumably more cemented, fractures. In contrast, larger aperture coefficient values indicate open fractures, which could form as a result of weak cementation, dissolution or in situ stresses (Lowell et al., 1993; Laubach et al., 2004; Barton, 2014; Bisdom et al., 2016; Deng et al., 2018).

The two major sections (upper part: 0–400 m; lower part: 400–915 m) of the well determined by the fracture density are also traceable along with the aperture coefficient and effective porosity logs. The aperture coefficients of the fractures vary significantly in the upper section, where well-cemented and poorly cemented sections probably alternate (Tokan-Lawal et al., 2017). The effective porosity varies depending on the change in the aperture coefficient; where the fractures are more open, the effective porosity increases. In the lower section, the aperture of the fractures decreases significantly. Two of the fracture zones in the lower part at 500 and 850 m have slightly increased aperture coefficients and effective porosity values. The fractures in these zones are probably less cemented. Deeper segments of the borehole generally have smaller aperture coefficients and effective porosity values. The highly fractured zone at 650 m determined by the P10 parameter (Fig. 5A) cannot be detected on either the aperture coefficient log or the effective porosity log. Based on this observation, this fracture zone probably contains well-cemented fractures that are less hydraulically active. Furthermore, this zone exemplifies that a dense fracture network does not automatically coincide with a hydraulically active system.

The hydraulic behaviour of the well can also be characterised by FZI, which concludes the relationship between porosity and permeability. Two different trends can be recognised along the well based on the poro-perm diagram. A significant part of the rock body aligns to a single trend, suggesting that the predominantly homogenous lithology of the BAF–2 well also has homogeneous hydrodynamic features.

There are three 60–100 m wide sections, where the data determine a different trend on the poro-perm plot and the coinciding FZI values also differ. All of these sections form independent hydraulic flow units along the well. Such deviations may be caused by changes in lithological or structural features.

5.3.1. Weathered HFU

The first hydraulic unit of the BAF–2 well with elevated FZI values appears between 60 and 110 m (Fig. 8C/a). In this section, the porosity decreases more considerably than the permeability, causing an increase in FZI. A possible explanation for this behaviour is that this section of the rock body is significantly altered by weathering, which is the result of the long-term near-surface position of the BCF. Limonite is present in the upper 100 m of the well that formed due to weathering of the haematite-bearing host rock by meteoric waters in the upper part of the rock body (Konrád et al., 2015). As the limonite density is approximately 2.7–4.3 g/cm^3 and that of haematite is 5.3 g/cm^3, hydration of the original rock-forming mineral phase is accompanied by a significant volume increase in the host rock. The volume increases from 30.28 to 41.64 cm^3 for each mole of haematite, which should cause a considerable reduction in the matrix porosity. Besides limonite, smectite and chlorite-smectite formed during weathering in the uppermost 100 m (Máthé, 2015). This alteration of clay minerals further reinforces the same tendency of porosity reduction. Permeability, which is mainly connected to structural elements, such as fractures and bedding planes, is less reduced due to the same hydration processes. Hence, limonite formation and the alteration of clay minerals greatly influenced the hydraulic behaviour of the rock body, allowing the development of a flow unit with increased FZI values in the uppermost zone of the well.

5.3.2. Sheared HFU

The second hydraulic flow unit, which differs from the primary FZI trend, occurs between 350 and 420 m (Fig. 8C/c). Along this section, the porosity is very low (Fig. 5D), but the permeability does not decrease to the same extent, resulting in elevated FZI values (Fig. 8C/c). At approximately 400 m, this depth interval appears as a boundary in several features along the well. Here, a significant drop in the fracture density is apparent (Fig. 5A), which alone should cause simultaneous decreases in porosity and permeability, but this would not change the FZI trend.

Nevertheless, the above calculations confirm that the aperture coefficient is substantially reduced in this depth interval. The anomalously low aperture coefficient values suggest that the fractures are more intensely closed than is typical in the well. Furthermore, a sharp decrease in the acoustic wave velocity is also observed below 400 m. This feature reflects the appearance of a rock body with significantly different rock mechanical properties, even if the lithology and the fracture geometry parameters (other than the density) do not change at this boundary. Furthermore, the presence of all four vein generations (Hrabovszki et al., 2017, 2020, 2022; Tóth et al., 2020) along the well suggests that the entire rock column shares an identical structural evolutionary history.

Konrád et al. (2015) explained that the difference between the upper (0–400 m) and lower (400–915 m) segments of the rock body developed during uplift of the formation and the coincident loosening of the upper section. Nevertheless, exhumation would result in a continuous transition in the fracture density and would not justify the observed pattern. The well-defined boundary may instead indicate lithological or structural changes. Based on sedimentological observations (changes in the style of graded bedding, overturned strata sections, etc.), a large-scale shear zone was previously assumed to be present around the same interval (Konrád et al., 2015), without the possibility of precisely locating it. Such a large-scale fault zone is difficult to detect using exclusively small-scale observations. Fault evolution in hard claystones starts with cataclasis, where clay gouges could fill the space between the initial fractures. As faulting progresses, a fully reworked clay gouge could form, which is often not accompanied by mineralogical changes. These evolutionary stages coexist in a fault zone (Holland et al., 2006). The separation of the lithotypes of a fault zone in the highly fractured BCF is

difficult, but the changes in porosity and transport properties could strongly indicate a fault zone (Holland et al., 2006).

The FZI log also draws this broad interval as an independent hydraulic flow unit. Above this HFU (350–420 m), the FZI values continuously deviate from the primary trend. Below this zone, FZI values continuously decrease forming a more than 100 m wide disturbed zone (Fig. 8C). Taking all observations into account, the entire flow unit with elevated FZI values can indicate the core and the damage zones of a large-scale fault zone. The low fracture density and low porosity in the core zone may be derived from the self-sealing properties of the claystone (Holland et al., 2006; Zhang, 2013; Rutqvist et al., 2020). The very low aperture coefficient values in the core zone also confirm this phenomenon. We propose a large-scale structural boundary at 400 m crosscut by the BAF–2 well. Considering all the above findings, a shear zone more than 100 m wide can be supposed at this interval in the rock body.

5.3.3. Coarse-grained HFU

The third section in the borehole with elevated FZI values appears between 690 and 770 m (Fig. 8C/e). At the boundary of the zone, FZI values change abruptly; unlike to the anomalous zones mentioned above, there is no continuous transition between the major trend and this HFU.

In this zone, the fracture density is not too high, but both the aperture coefficient and the porosity values are slightly elevated. Since sandstone layers become more frequent at this interval, the changes in the hydraulic properties of this section may be due to lithological reasons.

On the other hand, in this HFU the sonic log disturbance is similar to the behaviour observed at approximately 400 m (Fig. 2B). The acoustic wave velocity decreases significantly, especially between 680 and 690 m. The similarity of this pattern to the structural boundary at 400 m implies that another structural boundary is located at this depth. In this case, the core of the fault zone may be indicated by the lowest velocity of the acoustic waves between 680 and 690 m, and the highly fractured section may represent the damage zone (Holland et al., 2006).

At both margins of this HFU FZI are lowest within the whole rock column (FZI >200). Between 640 and 670 m (Fig. 8C), fracture density increases; one of the three fracture zones of the lower part of the well appears in this depth interval. This section could form a flow unit if we draw the lower limit of the main trend at 200 FZI values, but the poro-perm trend of these data points is very similar to the main trend. Therefore, it is just a matter of interpretation whether it is an independent unit or not. The lithology does not change significantly here, and the mineral compositions of the four vein generations are unchanged (Hrabovszki et al., 2017, 2020, 2022; Tóth et al., 2018, 2020). Therefore, this section could not have formed due to its unique lithology or a different history of vein formation. Nevertheless, this section contains well-cemented fractures, as indicated by the aperture coefficients and effective porosity logs mentioned above (Fig. 5C and D). The high fracture density in this section could enhance fluid flow, leading to a high degree of cementation (Lee et al., 1996). This process should result in decreasing permeability and low FZI values. As a result, this depth interval has the worst hydraulic properties of the entire well, despite being one of the highly fractured zones of the well.

This hydraulic unit could have formed due to the complex effects of several processes. Among them, the increasing number of coarse-grained beds and the impact of a possible structural boundary are the most emphasised.

5.4. Near-well fracture network geometry

The geometry of the fracture system corroborates the designated hydraulic units within the well. In some cases, the whole modelled fracture system defines one connected system. Therefore, the fracture geometry properties allow a more than 1000 m wide, hydraulically communicating fracture system (Fig. 7A).

In numerous fracture network models, connected fracture subgroups form and are usually separated at the well-defined depths mentioned above. These designated boundaries appear at approximately 100, 400 and 700 m. At these particular depths, the fracture system should be close to its percolation threshold; therefore, the fracture network connectivity cannot be predicted (Berkowitz, 1995; M. Tóth and Vass, 2011). Even small changes in the modelling parameters can significantly influence the connectivity between the subsystems. Even using the same parameter set may result in different fracture patterns in terms of connectivity (M. Tóth and Vass, 2011).

Taking the modelled fracture geometries together with the information from the hydraulic flow units, the rock body of the BAF–2 well can be divided into four blocks (Fig. 7E) with boundaries at approximately 100, 400 and 700 m. Around these boundaries, the rock body has specific hydraulic and rheological properties; otherwise, it behaves homogeneously from both physical aspects. Furthermore, all the blocks are affected by the main vein-forming events that developed the four vein generations of the well.

6. Conclusions

In this study, we examined the hydrological consequences of the fracture system of a claystone formation. A fundamental attribute of a fracture network is its spatial density, based on which the studied rock column can be divided into two major parts. The upper part of the BAF–2 well, between 0 and 400 m, is highly fractured, while the lower section, below 400 m, contains significantly fewer fractures on average. The lithology of the well is mostly homogenous; nevertheless, coarser-grained beds become more frequent with depth. The positions of the intensely fractured zones are primarily determined by tectonic processes, but the changing grain size could also influence the fracture density.

The hydraulic properties of the fracture system were investigated using measured permeabilities and computed effective porosities. For this calculation, aperture coefficients were estimated using DFN models for each depth interval where transmissivity measurements were available. The data evaluation suggests that two different poro-perm trends define the hydraulic behaviour of the rock body crosscut by the studied well. While most intervals conform to one trend, three sections differ from it and define distinct hydraulic flow units based on the FZI values.

The communicating fracture clusters and the hydraulic flow units designate the same horizons in the well. Considering the hydraulic characteristics and the fracture geometry, the rock body of the BAF–2 well could be divided into four blocks separated by boundaries at ~100, ~400 and ~700 m. The formation of the boundary at ~100 m is related to the alteration of the rock due to weathering. Another boundary at ~400 m probably represents the core zone of a wide shear zone. In comparison, the horizon at ~700 m could result from the combined effects of lithology and tectonic activity.

This study outlines the fracture network geometry and the hydraulic features of the BAF–2 well, which may provide a solid basis for further hydrodynamic modelling of the well and its surroundings.

Author statement

Emese Tóth: Writing- Original draft preparation, Visualization, Investigation, Conceptualization, Ervin Hrabovszki: Writing - Review & Editing, Félix Schubert: Conceptualization, Writing - Review & Editing Tivadar M. Tóth: Conceptualization, Methodology, Software, Supervision, Writing - Review & Editing.

Declaration of competing interest

The authors declare the following financial interests/personal relationships which may be considered as potential competing interests: Tivadar M. Tóth reports financial support was provided by National

Research Development and Innovation Office. Emese Tóth reports financial support was provided by University of Szeged Open Access Fund.

Acknowledgements

Access to the data of the BAF–2 well was provided by the Public Limited Company for Radioactive Waste Management (RHK Kft.) and the Mecsekérc Zrt. Zoltán Máthé is thanked for his comprehensive assistance. We thank the two anonymous reviewers whose comments helped improve and clarify this manuscript.

The research was financially supported by the National Research, Development and Innovation Office (grant no. K-138919) and the University of Szeged Open Access Fund (grant no. 5454).

References

Al-Dhafeeri, A.M., Nasr-El-Din, H.A., 2007. Characteristics of high-permeability zones using core analysis, and production logging data. J. Petrol. Sci. Eng. 55, 18–36. https://doi.org/10.1016/j.petrol.2006.04.019.

Amaefule, J.O., Altunbay, M., Tiab, D., Kersey, D.G., Kedan, D.K., 1993. Enhanced reservoir description: using core and log data to identify hydraulic (flow) unites and predict permeability in uncored intervals/wells. In: SPE 26436. SPE Annual Technical Conference and Exhibition, Houston, Texas. https://doi.org/10.2118/26436-MS.

Anders, M.H., Laubach, S.E., Scholz, C.H., 2014. Microfractures: a review. J. Struct. Geol. 69, 377–394. https://doi.org/10.1016/j.jsg.2014.05.011.

Andrássy, M., Dankó, Gy, Darvas, K., Farkas, M.P., Korpai, F., Talpas, L., 2018. Hydrofracking and hydraulic packer testing in the framework of Boda Claystone Formation (BCF) geological investigation program in the Kővágószőlős southern anticline tectonic block. In: Bodai Agyagkő Formáció Kutatás Szakmai Előadói Nap Kiadványa (Lecture Day of the Boda Claystone Formation Research). Pécs (in Hungarian).

Árkai, P., Demény, A., Fórizs, I., Nagy, G., Balogh, K., Máthé, Z., 2000. Composition, diagenetic and post-diagenetic alterations of a possible radioactive waste repository site: the Boda Albitic claystone formation, southern Hungary. Acta Geol. Hung. 43, 351–378.

Barton, N., 2014. Non-linear behaviour for naturally fractured carbonates and frac-stimulated gas-shales. First Break 32/2031, 51–66. https://doi.org/10.3997/1365-2397.2014011.

Barton, C.C., Larsen, E., 1985. Fractal geometry of two-dimensional fracture networks at Yucca Mountain, Southwestern Nevada. In: Stephanson, O. (Ed.), Proceedings of International Symposium on Fundamentals of Rock Joints 77–84.

Bauer, M., M. Tóth, T., 2017. Characterization and DFN modelling of the fracture network in a Mesozoic karst reservoir: gomba oilfield, Paleogene Basin, Central Hungary. J. Petrol. Geol. 40/3, 319–334. https://doi.org/10.1111/jpg.12678.

Benkovics, L., Mansy, J.-L., Csontos, L., Bergerat, F., 1997. Folding in the Abaliget road cut (Mecsek mountains). Acta Geol. Hung. 40/4, 425–440.

Bergerat, F., Csontos, L., 1988. Brittle tectonics and paleo-stress field in the Mecsek and Villány Mts (Hungary): correlation with the opening mechanism of the Pannonian Basin. Acta Geol. Hung. 31, 81–100.

Berkowitz, B., 1995. Analysis of fracture network connectivity using percolation theory. Math. Geol. 27/4, 467–483. https://doi.org/10.1007/BF02084422.

Bernáth, Gy, 2015. Lyukgeofizikai értékelés. In: Sámson, M. (Ed.), BAF–2 Fúrás Dokumentáló És Értékelő Jelentése. (Documentation and Evaluation of the BAF–2 Well). Research Report, Public Limited Company for Radioactive Waste Management (RHK Kft.), Pécs (in Hungarian), 2015.

Bernáth, Gy, Gärtner, D., Zilahi-Sebess, L., Prohászka, A., Hegedűs, S., 2014. A BAF–2 jelű magfúrás mélyfúrás-geofizikai dokumentálása és értékelése (Geophysical documentation and evaluation of the BAF–2 well). Research Report. Geo-Log Környezetvédelmi és Geofizikai Kft., Budapest (in Hungarian).

Bisdom, K., Bertotti, G., Nick, H., 2016. A geometrically based method for predicting stress-induced fracture aperture and flow in discrete fracture networks. AAPG (Am. Assoc. Pet. Geol.) Bull. 100, 1075–1097. https://doi.org/10.1306/02111615127.

Brace, W.F., Riley, D.K., 1972. Static uniaxial deformation of 15 rocks to 30 kb. Int. J. Rock Mech. Min. Sci. 9, 271–288. https://doi.org/10.1016/0148-9062(72)90028-9.

Cheng, C., Hale, S., Milsch, H., Blum, P., 2020. Measuring hydraulic fracture apertures: a comparison of methods. Solid Earth 11, 2411–2423. https://doi.org/10.5194/se-11-2411-2020.

Childs, C., Walsh, J.J., Watterson, J., 1997. Complexity in fault zone structure and implication for fault seal prediction. In: Moller-Pedersen, P., Koestler, A.G. (Eds.), Hydrocarbon Seals. Elsevier. https://doi.org/10.1016/S0928-8937(97)80007-0.

Csicsák, J., 1999. Hidrológiai, Hidrokémiai Vizsgálati Program (Hydrological, Hydrochemical Study). Research Report, Mecsekérc Zrt., Pécs (in Hungarian).

Csontos, L., Bergerat, F., 1992. Reevaluation of the Neogene brittle tectonics of the Mecsek–Villány are (SW Hungary). In: Annales Universitatis Scientiarum Budapestinensis de Rolando Eötvös Nominatae, vol. 29, pp. 3–12. Sectio geologica.

Csontos, L., Benkovics, L., Bergerat, F., Mansy, J.-L., Wórum, G., 2002. Tertiary deformation history from seismic section study and fault analysis in a former European Tethyan margin (the Mecsek–Villány area, SW Hungary). Tectonophysics 357, 81–102. https://doi.org/10.1016/S0040-1951(02)00363-3.

Deng, H., Steefel, C., Molins, S., DePaolo, D., 2018. Fracture evolution in Multimineral systems: the role of mineral composition, flow rate, and fracture aperture heterogeneity. Earth Space Chem. 2/2, 112–124. https://doi.org/10.1021/acsearthspacechem.7b00130.

Dezfoolian, M.A., 2013. Flow zone indicator estimation based on petrophysical studies using an artificial neural network in a southern Iran reservoir. Petrol. Sci. Technol. 31 (12), 1294–1305. https://doi.org/10.1080/10916466.2010.542421.

Fodor, L., Csontos, L., Bada, G., Györfi, I., Benkovics, L., 1999. Tertiary tectonic evolution of the Pannonian Basin system and neighbouring orogens: a new synthesis of palaeostress data. In: Durand, B., Jolivet, L., Horváth, F., Séranne, M. (Eds.), The Mediterranean Basins: Tertiary Extension within the Alpine Orogen, vol. 156. Geological Society, London, Special Publications, pp. 295–334. https://doi.org/10.1144/GSL.SP.1999.156.01.15.

Grant, S.A., 2005. Hydraulic properties, temperature effects. In: Hillel, D. (Ed.), Encyclopedia of Soils in the Environment. Elsevier, pp. 207–211.

Gudmundsson, A., Berg, S.S., Lyslo, K.B., Skurtveit, E., 2001. Fracture networks and fluid transport in active fault zones. J. Struct. Geol. 23 (2/3), 343–353. https://doi.org/10.1016/S0191-8141(00)00100-0.

Holland, M., Urai, J.L., van derZee, W., Stanjek, H., Konstanty, J., 2006. Fault gouge evolution in highly overconsolidated claystones. J. Struct. Geol. 28/2, 323–332. https://doi.org/10.1016/j.jsg.2005.10.005.

Hrabovszki, E., Tóth, E., Raucsik, B., Varga, A., Schubert, F., 2017. Microstructure and cementation analyses on core samples from the BAF–2 well (Boda claystone formation, Mecsek Mts). Bull. Hungar Geol. Soc. 147/3, 245–264. https://doi.org/10.23928/foldt.kozl.2017.147.3.245 (in Hungarian with English abstract).

Hrabovszki, E., Tóth, E., M. Tóth, T., Máthé, Z., Schubert, F., 2020. Potential formation mechanisms of early diagenetic displacive veins in the Permian Boda Claystone Formation. J. Struct. Geol. 138, 104098. https://doi.org/10.1016/j.jsg.2020.104098.

Hrabovszki, E., Tóth, E., M. Tóth, T., Garaguly, I., Futó, I., Máthé, Z., Schubert, F., 2022. Geochemical and microtextural properties of veins in a potential high-level radioactive waste disposal site. J. Struct. Geol. 154, 104490. https://doi.org/10.1016/j.jsg.2021.104490.

Keller, A., 1998. High resolution, non-destructive measurement and characterization of fracture apertures. Int. J. Rock Mech. Min. Sci. 35/8, 1037–1050. https://doi.org/10.1016/S0148-9062(98)00164-8.

Konrád, Gy, Hámos, G., 2006. Geological aspects of determining high activity radioactive waste depository sites in Hungary and the results of the recent research. Acta Geogr. Geol. Meteorol. Debrecina 1, 33–38.

Konrád, Gy, Sebe, K., 2010. New details of young tectonic phenomena in the Western Mecsek Mts and their surroundings. Bull. Hungar Geol. Soc. 140, 135–162 (in Hungarian with English abstract).

Konrád, Gy, Sebe, K., Halász, A., Babinszki, E., 2010. Sedimentology of a Permian playa lake: the Boda claystone formation, Hungary. Geologos 16, 27–41. https://doi.org/10.2478/v10118-010-0002-1.

Konrád, Gy, Sebe, K., Halász, A., 2015. Földtani-tektonikai értékelés. In: Sámson, M. (Ed.), BAF–2 Fúrás Dokumentáló És Értékelő Jelentése. (Documentation and Evaluation of the BAF–2 Well). Research Report, Public Limited Company for Radioactive Waste Management (RHK Kft.), Pécs (in Hungarian), 2015.

Krauskopf, K.B., 1988. Radioactive Waste Disposal and Geology. Springer, Dordrecht. https://doi.org/10.1007/978-94-009-1201-4.

Kumar, S., Bodvarsson, G.S., Boernge, J., 1991. Fractal characteristics of fracture roughness and aperture data. In: High-Level Nuclear Waste Management, Proceedings of the Second International Conference. Las Vegas, Nevada, pp. 279–284.

La Pointe, P.R., 1988. A method to characterize fracture density and connectivity through fractal geometry. Int. J. Rock. Mech. Min. Sci. Geomech. Abstr. 25, 421–429. https://doi.org/10.1016/0148-9062(88)90982-5.

Laubach, S.E., Olson, J.E., Gale, J.F., 2004. Are open fractures necessarily aligned with maximum horizontal stress? Earth Planet Sci. Lett. 222 (1), 191–195. https://doi.org/10.1016/j.epsl.2004.02.019.

Lee, Y.J., Morse, J.W., Wlitschko, D.V., 1996. An experimentally verified model for calcite precipitation in veins. Chem. Geol. 130, 203–215. https://doi.org/10.1016/0009-2541(96)00008-3.

Liu, E., 2005. Effects of fracture aperture and roughness on hydraulic and mechanical properties of rocks: implication of seismic characterization of fractured reservoirs. J. Geophys. Eng. 2 (1), 38–47. https://doi.org/10.1088/1742-2132/2/1/006.

Lowell, R.P., Van Cappellen, P., Germanovich, L.N., 1993. Silica precipitation in fractures and the evolution of permeability in hydrothermal upflow zones. Science 260, 192–194. https://doi.org/10.1126/science.260.5105.192.

M. Tóth, T., 2010. Determination of geometric parameters of fracture networks using 1D data. J. Struct. Geol. 32, 878–885. https://doi.org/10.1016/j.jsg.2009.04.006.

M. Tóth, T., 2018. Fracture network characterisation using 1D and 2D data of the Mórágy Granite body, Southern Hungary. J. Struct. Geol. 113, 176–187. https://doi.org/10.1016/j.jsg.2018.05.029.

M. Tóth, T., Hollós, Cs, Szűcs, É., Schubert, F., 2004. Conceptual fracture network model of the crystalline basement of the Szeghalom Dome (Pannonian Basin, SE Hungary). Acta Geol. Hung. 47/1, 19–34. https://doi.org/10.1556/AGeol.47.2004.1.2.

M. Tóth, T., Vass, I., 2011. Relationship between the geometric parameters of rock fractures, the size of percolation clusters and REV. Math. Geosci. 43, 75–97. https://doi.org/10.1007/s11004-010-9315-4.

Maros, Gy, Koroknai, B., Palotás, K., Fodor, L., Dudko, A., Forián-Szabó, M., Zilahi-Sebess, L., Bán-Győri, E., 2004. Tectonic Analysis and Structural Evolution of the North-Eastern Mórágy Block. Annual Report of the Geological Institute of Hungary, pp. 371–386, 2003.

Máthé, Z., 2015. Results of Mineralogical, Petrological and Geochemical Investigation of Boda Claystone Formation. Doctoral dissertation Eötvös Lóránd University, Budapest, Hungary (in Hungarian with English summary).

Min, K.B., Jing, L., Stephansson, O., 2004. Determining the equivalent permeability tensor for fractured rock masses using a stochastic REV approach: method and application to the field data from Sellafield, UK. Hydrogeol. J. 12 (5), 497–510. https://doi.org/10.1007/s10040-004-0331-7.

National Research Council, 1996. Rock fractures and fluid flow: contemporary understanding and applications. In: Chapter: 2 Physical Characteristics of Fractures and Fracture Patterns. The National Academies Press, Washington, DC. https://doi.org/10.17226/2309.

Németh, T., Máthé, Z., Pekker, P., Dódony, I., Kovács-Kis, V., Sipos, P., Cora, I., Kovács, I., 2016. Clay mineralogy of the Boda claystone formation (Mecsek Mts., SW Hungary). Open Geosci. 8/1, 259–274. https://doi.org/10.1515/geo-2016-0024.

Neuzil, C.E., Tracy, J.V., 1981. Flow through fractures. Water Resour. Res. 17/1, 191–199. https://doi.org/10.1029/WR017i001p00191.

Olsson, R., Barton, N., 2001. An improved model for hydromechanical coupling during shearing of rock joints. Int. J. Rock Mech. Min. Sci. 38 (3), 317–329. https://doi.org/10.1016/S1365-1609(00)00079-4.

Opheim, J.A., Gudmundsson, A., 1989. Formation and geometry of fractures, and related volcanism, of the Krafla fissure swarm, northeast Iceland. Bull. Geol. Soc. Am. 101, 1608–1622. https://doi.org/10.1130/0016-7606(1989)101<1608:FAGOFA>2.3.CO;2.

Paillet, F.L., Kay, R.T., Yeskis, D., Pedler, W., 1993. Integrating well logs into a multi-scale investigation of a fractured sedimentary aquifer. Log. Anal. 34 (1), 13–23.

Paterson, M.S., 1978. In: Experimental Rock Deformation: the Brittle Field. Springer, Berlin. https://doi.org/10.1007/b137431.

Pollard, D.D., Segall, P., 1987. Theoretical displacements and stresses near fractures in rock: with application to faults, joints, veins, dikes and solution surfaces. In: Atkinson, B. (Ed.), Fracture Mechanics of Rock. Academic Press, London. https://doi.org/10.1016/C2009-0-21691-6.

Rutqvist, J., Graupner, B., Guglielmi, Y., Kim, T., Maßmann, J., Nguyen, T.S., Jung-Wook Park, J.W., Shiu, W., Urpi, L., Yoon, J.S., Ziefle, G., Birkholzer, J., 2020. An international model comparison study of controlled fault activation experiments in argillaceous claystone at the Mont Terri Laboratory. Int. J. Rock Mech. Min. Sci. 136, 104505. https://doi.org/10.1016/j.ijrmms.2020.104505.

Sebe, K., 2017. Structural evolution of the Mecsek–Villány area (SW Hungary) during post-rift phase and basin inversion. In: Horvat, M., Wacha, L. (Eds.), 7th International Workshop "Neogene of Central and South-Eastern Europe". Velika, Croatia.

Tokan-Lawal, A., Prodanović, M., Landry, C.J., Eichubl, P., 2017. Influence of numerical cementation on multiphase displacement in rough fractures. In: Transport in Porous Media 116/1, pp. 275–293. https://doi.org/10.1007/s11242-016-0773-0.

Tóth, E., Hrabovszki, E., Steinbach, G., Schubert, F., 2018. Quantitative estimation of shear strain and volume change using sigmoidal tension gashes. Bull. Hungar Geol. Soc. 148/4, 367–380. https://doi.org/10.23928/foldt.kozl.2018.148.4.367 (in Hungarian with English abstract).

Tóth, E., Hrabovszki, E., M. Tóth, T., Schubert, F., 2020. Shear strain and volume change associated with sigmoidal vein arrays in the Boda Claystone. J. Struct. Geol. 138, 104105. https://doi.org/10.1016/j.jsg.2020.104105.

Turcotte, D.L., 1992. Fractals and Chaos in Geology and Geophysics. Cambridge University Press. https://doi.org/10.1002/gj.3350280216.

Varga, A., 2009. Petrology and Geochemistry of the Paleozoic–Lower Triassic Siliciclastic Rocks from Southern Transdanubia, Hungary. PhD thesis. Eötvös Loránd University (in Hungarian with English summary).

Varga, A., Szakmány, Gy, Raucsik, B., Máthé, Z., 2005. Chemical composition, provenance and early diagenetic processes of playa lake deposits from the Boda Siltstone Formation (Upper Permian), SW Hungary. Acta Geol. Hung. 48, 49–68. https://doi.org/10.1556/AGeol.48.2005.1.2.

Varga, A., Raucsik, B., Szakmány, Gy, Máthé, Z., 2006. Mineralogical, petrological and geochemical characteristics of the siliciclastic rock types of Boda Siltstone Formation. Bull. Hungar Geol. Soc. 136/2, 201–231 (in Hungarian with English abstract).

Vermilye, J.M., Scholz, C.H., 1995. Relation between vein length and aperture. J. Struct. Geol. 17/3, 423–434. https://doi.org/10.1016/0191-8141(94)00058-8.

Witherspoon, P.A., Wang, J.S.Y., Iwai, K., Gale, J.E., 1980. Validity of cubic law for fluid flow in deformable rock fracture. Water Resour. Res. 16/6, 1016–1024. https://doi.org/10.1029/WR016i006p01016.

Yielding, G., Walsh, J.J., Watterson, J., 1992. The prediction of small scale faulting in reservoirs. First Break 10, 449–460. https://doi.org/10.3997/1365-2397.1992023.

Zhang, C.L., 2013. Sealing of fractures in claystone. J. Rock Mech. Geomech. Eng. 5 (3), 214–220. https://doi.org/10.1016/j.jrmge.2013.04.001.

Zimmerman, R.W., Bodvarsson, S., 1996. Hydraulic conductivity of rock fractures. Transport in Porous Media 23/1. https://doi.org/10.1007/BF00145263, 1-30.